

Collisional excitation of NH_3 by atomic and molecular hydrogen

N. Bouhafs¹, C. Rist², F. Daniel², F. Dumouchel¹, F. Lique¹, L. Wiesenfeld²
and A. Faure^{2*}

¹ *Université Normandie, CNRS, LOMC, F-76058 Le Havre, France*

² *Université Grenoble Alpes, CNRS, IPAG, F-38000 Grenoble, France*

29 November 2018

ABSTRACT

We report extensive theoretical calculations on the rotation-inversion excitation of interstellar ammonia (NH_3) due to collisions with atomic and molecular hydrogen (both para- and ortho- H_2). Close-coupling calculations are performed for total energies in the range $1\text{--}2000\text{ cm}^{-1}$ and rotational cross sections are obtained for all transitions among the lowest 17 and 34 rotation-inversion levels of ortho- and para- NH_3 , respectively. Rate coefficients are deduced for kinetic temperatures up to 200 K. Propensity rules for the three colliding partners are discussed and we also compare the new results to previous calculations for the spherically symmetrical He and para- H_2 projectiles. Significant differences are found between the different sets of calculations. Finally, we test the impact of the new rate coefficients on the calibration of the ammonia thermometer. We find that the calibration curve is only weakly sensitive to the colliding partner and we confirm that the ammonia thermometer is robust.

Key words: Molecular data, Molecular processes, scattering.

1 INTRODUCTION

Ammonia (NH_3) was the first polyatomic molecule to be detected in the interstellar medium (ISM) by Cheung et al. (1968). NH_3 is an ubiquitous molecule in the ISM and an invaluable probe of the physical conditions thanks to its many observable transitions that are sensitive to excitation conditions. NH_3 has been detected in a large variety of interstellar environments, ranging from pre-stellar cores to external galaxies (Ho & Townes 1983).

With the launch of the far-infrared Herschel Space Observatory in 2009, new opportunities have been created to perform observations of NH_3 , together with other related nitrogen hydrides such as NH and NH_2 . These observations have allowed a new insight into the interstellar nitrogen chemistry. For example, Le Gal et al. (2014) have derived $\text{NH}:\text{NH}_2:\text{NH}_3$ abundance ratios of 3:1:19 towards the external envelope of the protostar IRAS16293. Towards diffuse interstellar clouds, Persson et al. (2010) have obtained a similar $\text{NH}:\text{NH}_2$ ratio of 2:1 but a much larger $\text{NH}_2:\text{NH}_3$ ratio of $\sim 1:1$. NH_3 also exhibits nuclear spin symmetry states whose relative abundances have been measured in the cold diffuse gas with Herschel (Persson et al. 2012). The derived

anomalous (non-thermal) NH_3 ortho-to-para ratio (OPR) of ~ 0.6 was shown to reflect the small H_2 OPR ($\lesssim 10^{-3}$) in the gas phase (Faure et al. 2013).

Ammonia has always been recognized as a good thermometer (Walmsley & Ungerechts 1983) because the relative populations of the metastable levels $j = k$ (where j is the total angular momentum quantum number of NH_3 , and k is the projection of j on the C_3 rotational axis) involved in the inversion transitions are mainly determined by collisional processes. In addition, as these transitions arise from quite different energy levels but take place in a narrow wavelength window close to 1.3 cm, they can be probed by a single telescope and receiver, i.e. at the same spectral and spatial resolution and with small relative calibration errors. The calibration of the ammonia thermometer however depends critically on the accuracy of the collisional rate coefficients.

The collisional excitation of NH_3 has been the object of numerous studies since the late 1960s. Following the pioneering double resonance experiments on $\text{NH}_3\text{--He}$ performed by Oka (1967), the first theoretical study of ammonia inelastic collisions with He was investigated by Green (1976). An electron gas approximation of the potential energy surface (PES) was employed and the quantal dynamical formalism was introduced for the first time for the excitation of a symmetric top molecule by a spherical atom, with the inclu-

* E-mail: alexandre.faure@univ-grenoble-alpes.fr

sion of the inversion motion. The first scattering calculations for NH_3 in collision with para- $\text{H}_2(j_2 = 0)$ (hereafter the H_2 rotational states are denoted by j_2) were performed in the 1980s by Danby et al. (1988) based on the PES of Danby et al. (1986). The derived rate coefficients were employed to recalibrate the ammonia thermometer which was previously based on $\text{NH}_3\text{-He}$ rate coefficient calculations. The accuracy of the PES of Danby et al. (1986) was later checked against pressure broadening measurements at low temperature (12.5–40 K) and a good agreement was found between theory and experiment (Willey et al. 2002). It was also shown that broadening cross sections involving para- $\text{H}_2(j_2 = 0)$ were up to four times larger than those obtained with He.

Revised collisional rate coefficients for NH_3 colliding with He and para- $\text{H}_2(j_2 = 0)$ were computed recently using improved PESs. The $\text{NH}_3\text{-He}$ PES of Hodges & Wheatley (2001), generated using scaled perturbation theory calculations, was employed by Machin & Roueff (2005) to perform quantal close-coupling and approximate coupled-states scattering calculations. Their cross sections were compared to the crossed beam measurements of Schleipen & ter Meulen (1991) at a relative kinetic energy of 436 cm^{-1} . The agreement between the theoretical parity averaged cross sections and the experimental data was found to be satisfactory but significant discrepancies were observed for some parity-resolved state-to-state cross sections. Rate coefficients were obtained for kinetic temperatures ranging from 5 to 300 K and for transitions up to $j = 4$ for para- NH_3 , and up to $j = 7$ for ortho- NH_3 . An improved $\text{NH}_3\text{-He}$ PES was also obtained more recently by Gubbels et al. (2012) using a coupled-cluster method, from which cross sections (but no rate coefficients) were computed. A very satisfactory agreement was obtained with this PES between theoretical and experimental state-to-state differential cross sections (DCSs) (Tkáč et al. 2014).

The revised $\text{NH}_3\text{-para-H}_2(j_2 = 0)$ rate coefficients were computed by Maret et al. (2009) at the full close-coupling level using a new PES computed at the coupled cluster level. The $\text{NH}_3\text{-para-H}_2(j_2 = 0)$ rate coefficients were found in good agreement with the previous calculations by Danby et al. (1988) (within a factor of 2) and significant differences with the $\text{NH}_3\text{-He}$ system were found. Rate coefficients were deduced for transitions among ammonia levels with $j \leq 3$ and kinetic temperatures in the range 5–100 K. It should be noted that the accuracy of the $\text{NH}_3\text{-H}_2$ PES of Maret et al. (2009) was recently checked against various experiments. In particular, state-to-state resolved DCSs for the inelastic scattering of ND_3 with H_2 at a collision energy of 580 cm^{-1} were measured by Tkáč et al. (2015) and satisfactorily reproduced by quantal calculations. The isotropic part of the $\text{NH}_3\text{-H}_2$ PES was also probed by the molecular beam experiment of Pirani et al. (2013), which has provided a further accuracy assessment by measuring the glory quantum interference structure. Finally, the rotational spectrum of the $\text{NH}_3\text{-H}_2$ van der Waals complex was measured very recently by Surin et al. (2017) and the deduced rotational constants were found to agree within 1–2% with those predicted from the PES of Maret et al. (2009). The overall agreement between theory and experiment for the $\text{NH}_3\text{-He}$ and $\text{NH}_3\text{-H}_2$ systems is an important testimony of the good accuracy of the most recent available PESs.

The story of ammonia excitation, however, is not over yet. Indeed, none of the above $\text{NH}_3\text{-H}_2$ studies have considered so far the rotational structure of H_2 . In the calculations of both Danby et al. (1988) and Maret et al. (2009), H_2 was restricted to its (spherically symmetrical) para $j_2 = 0$ state. As a result, there is no rate coefficient available for collisions with ortho- H_2 , even if some ortho- H_2 cross sections were computed at a few selected energies (Offer & Flower 1989; Rist, Alexander & Valiron 1993) with the PES of Danby et al. (1986). In addition, the calculations of Maret et al. (2009) for para- H_2 need to be improved by including $j_2 = 2$ in the scattering basis set. Finally, to the best of our knowledge, there is no collisional data available for collisions of NH_3 with H, which are of great importance in molecular gas with a low H_2 fraction.

In this paper, we provide new $\text{NH}_3\text{-H}_2$ calculations taking into account the rotational (non-spherical) structure of H_2 , using the $\text{NH}_3\text{-H}_2$ PES of Maret et al. (2009). Similar calculations were recently performed for the NH_3 deuterated isotopologues (i.e. NH_2D , NHD_2 and ND_3) by Daniel et al. (2014, 2016). The data of Maret et al. (2009) are also extended to higher temperatures. In addition, we provide the first set of rate coefficients for the $\text{NH}_3\text{-H}$ collisional system. For these calculations, we use the accurate full-dimensional NH_4 PES of Li & Guo (2014) which was recently employed in a $\text{NH}_2\text{-H}_2$ scattering study (Bouhafs et al. 2017).

The paper is organized as follow: The PESs and the scattering calculations are presented in Section 2. In section 3, we report state-to-state cross sections and rate coefficients for the rotational excitation of NH_3 by H and H_2 . The consequences for the ammonia thermometer are discussed in section 4. Concluding remarks are drawn in Section 5.

2 METHODS

2.1 Potential energy surface

The $\text{NH}_3\text{-H}_2$ PES was computed at the coupled cluster with single, double, and perturbative triple excitations [CCSD(T)] level of theory with a basis set extrapolation procedure, as described in Maret et al. (2009) where full details can be found. The ammonia and hydrogen molecules were both assumed to be rigid, which is justified at kinetic temperatures lower than $\sim 1000\text{ K}$ since the lowest vibrational mode of NH_3 opens at 950 cm^{-1} . The ammonia “umbrella” (inversion) motion was thus not described in the PES which depends on five coordinates only: the intermolecular distance R between the centers of mass of NH_3 and H_2 and four orientation angles. The NH_3 and H_2 geometries were taken at their ground-state averaged values: $r_{\text{NH}}=1.9512 a_0$, $\widehat{\text{H}}\text{NH}=107.38^\circ$ and $r_{\text{HH}}=1.4488 a_0$. A total of 118,000 *ab initio* points were computed by Maret et al. (2009). These grid points were chosen for 29 intermolecular distances (in the range 3–15 a_0) via random sampling for the angular coordinates. At each intermolecular distance, the interaction energy was least-squares fitted, using a 167-term expansion including anisotropies up to $l_1=10$ and $l_2=4$, where the integer indices l_1 and l_2 refer to the NH_3 and H_2 angular dependence, respectively. These 167 expansion terms were selected using a Monte Carlo error estimator defined in Rist & Faure (2012). The root mean squared error (RMSE) is lower than

1 cm⁻¹ for $R > 5 a_0$. A cubic spline interpolation was finally employed over the intermolecular distance grid and it was smoothly connected with standard extrapolations to provide continuous radial expansion coefficients. We note that this fit is different from that performed by Maret et al. (2009) because the potential expansion is expressed here in the body-fixed coordinates adapted to the HIBRIDON scattering code, as in Ma et al. (2015), whereas the MOLSCAT scattering code (Hutson & Green 1994) was employed by Maret et al. (2009). The global minimum deduced from our fit, lies at -267 cm⁻¹ for $R = 6.1 a_0$, with H₂ colinear with the C₃ axis of ammonia at the nitrogen end. This result can be compared with other recent calculations: Mladenović et al. (2008) and Sheppelman et al. (2012) found the global minimum at a similar location but with smaller binding energies of -253 cm⁻¹ and -245 cm⁻¹, respectively.

The NH₃-H PES was constructed from the recently computed nine-dimensional global PES of the ground electronic state of NH₄, as described by Li & Guo (2014) where full details can be found. This global PES was determined at the explicitly correlated unrestricted coupled-cluster level of theory using an augmented correlation-consistent triple zeta basis set (UCCSD(T)-F12a/aug-cc-pVTZ). The abstraction and exchange channels, respectively NH₃+H ↔ NH₂ + H₂ and NH₃+H ↔ NH₄ ↔ NH₃ + H, are thus included in the PES. They can be safely neglected here, because they involve energy barriers higher than 3200 cm⁻¹, which is much higher than the investigated collision energies¹. About 100,000 *ab initio* points were computed by Li & Guo (2014) and they were fitted using the permutation-invariant polynomial neutral network (PIP-NN) method with a RMSE of 27 cm⁻¹. The RMSE of 27 cm⁻¹ is for the full nine-dimensional PES (including the reactive path). The fitting RMSE for the non-reactive NH₃-H region relevant for this work is much smaller, of the order of a few cm⁻¹. In this work, NH₃ is considered as rigid with the ground-state averaged geometry of ammonia given above. The NH₃-H PES is thus described as a function of three coordinates: the distance R between the center of mass of NH₃ and the H atom, and two spherical angles. As the original routine of Li & Guo (2014) employs internuclear coordinates, the spherical to cartesian transformation was employed to determine the cartesian positions of the H atom in the ammonia body-fixed frame (see Bouhafs et al. (2017) for the general transformation in NH₂-H₂). The original fit of Li & Guo (2014) was employed to generate interaction energies on a dense grid of 90,000 geometries, chosen for 30 distances R (in the range 3–20 a_0) via random sampling for the angular coordinates. An asymptotic potential of 228.297 cm⁻¹ (corresponding to the above monomer averaged geometries) was subtracted from these interaction energies. At each intermolecular distance, the interaction energy was least-squares fitted, using a 26-term expansion including all anisotropies up to $l_1=10$. The RMSE is lower than 1 cm⁻¹ for $R > 4 a_0$. The global minimum, as deduced from our fit, lies at -78.31 cm⁻¹ for $R = 6.2 a_0$, with the H atom close to the equatorial location (16° below) and equidistant

from the two closest H atoms of ammonia. Similar equilibrium geometries were found for the minima in the NH₃-He and NH₃-para-H₂ ($j_2 = 0$) PES, with corresponding energies of -35.08 cm⁻¹ (Gubbels et al. 2012) and -85.7 cm⁻¹ (Maret et al. 2009), respectively.

2.2 Scattering calculations

The rotation-inversion levels of the NH₃ symmetric top molecules are labeled as j_k^ϵ , where j is the total angular momentum quantum number of the molecule, k is the projection of j on the C₃ axis and $\epsilon = \pm$ is the symmetry index. For each rotational state j_k^ϵ , the umbrella inversion symmetry is equal to $-(-1)^j \epsilon$ and the parity index of the rotation-inversion wave function is $-\epsilon(-1)^{j+k}$ (Rist, Alexander & Valiron 1993). Because of the symmetry under permutation of the three identical protons, the rotational states are split into two k stacks : ortho-NH₃ which correspond to $k=3n$ (with n an integer) and para-NH₃ with $k \neq 3n$ (hereafter denoted as o-NH₃ and p-NH₃ respectively). As for NH₃ the rotational states of H₂ molecule split into para and ortho nuclear-spin permutation symmetry modifications. The para states of H₂ have even rotational states $j_2 = 0, 2, \dots$ and the ortho states have odd rotational states, $j_2 = 1, 3, \dots$ (hereafter p-H₂ and o-H₂, respectively).

Since the umbrella inversion motion of the NH₃ molecule is not described in the PES (see above), the inversion-tunnelling wavefunctions were approximated as even and odd combination of the two rigid structures, as first suggested by Green (1976). Previous studies of the inelastic scattering of NH₃ by He and Ar atoms have demonstrated that this approximation is in very good agreement (i.e. better than 10%) with an elaborate treatment of the umbrella motion (e.g. Gubbels et al. 2012).

We used the rotational constants $A=B=9.9402$ cm⁻¹ and $C=6.3044$ cm⁻¹ for NH₃ and $B_0=59.3801$ cm⁻¹ for H₂. The experimental ground state inversion splitting of 0.7903 cm⁻¹ was also included. The reduced masses of the NH₃-H₂ and NH₃-H systems are 1.802 and 0.952 amu, respectively.

As the ortho and para levels of NH₃ and H₂ do not interconvert in inelastic collisions, these were treated separately. All calculations were performed using the HIBRIDON scattering code. The scattering equations were solved using the almost exact close-coupling approach. In the case of NH₃-H₂, the 167-term PES expansion (including anisotropies up to $l_1=10$ and $l_2=4$) was reduced in order to save computational time. In the close-coupling calculations, we thus adopted a 55-terms expansion including anisotropies up to $l_1=6$ and $l_2=2$. In the case of NH₃-H, all 26 terms of the PES expansion were used.

Scattering calculations were performed for total energies up to 1600 cm⁻¹ for NH₃-H₂ and up to 2000 cm⁻¹ for NH₃-H. We computed inelastic cross sections between levels with an internal energy lower than 419 cm⁻¹, that is up to $j_k=6_0$ for o-NH₃ and $j_k=6_1$ for p-NH₃. For collisions with p-H₂, the $j_2=0$ and $j_2=2$ levels of H₂ are included in the basis set, while for o-H₂ collisions, only the $j_2=1$ level was retained. For both collisional partners, the NH₃ rotational basis set also included several closed (or higher than 419 cm⁻¹) energy levels. Thus, at the highest investigated total energies and for collisions with H₂, the basis set included all

¹ The abstraction reaction is slow, with a rate coefficient lower than 10^{-15} cm³s⁻¹ at temperatures lower than 500 K (Li & Guo 2014)

levels with $j \leq 10$ and 12 for o- and p-NH₃, respectively. For collisions with H, the NH₃ basis set included all levels with $j \leq 9$ for o- and p-NH₃. These NH₃ and H₂ rotational basis sets allow the determination of cross sections converged within 10% accuracy. The integration parameters were also chosen to ensure convergence of the cross sections within a few percent. An energy step of 0.1 cm⁻¹ was used at low energies to properly describe resonances. This energy step has been progressively increased with increasing collision energy.

Finally, rate coefficients were obtained by integrating the cross sections over a Maxwell-Boltzmann distribution of relative velocities:

$$k_{\alpha \rightarrow \beta}(T) = \left(\frac{8}{\pi \mu k_B^3 T^3} \right)^{\frac{1}{2}} \times \int_0^{\infty} \sigma_{\alpha \rightarrow \beta} E_c e^{-\frac{E_c}{k_B T}} dE_c \quad (1)$$

where $\sigma_{\alpha \rightarrow \beta}$ is the cross section from the initial state α to the final state β , μ is the reduced mass of the system and k_B is the Boltzmann's constant. The range of total energies mentioned above allowed us to determine rate coefficients up to 200 K.

3 RESULTS

3.1 Cross sections

Figure 1 shows the collisional energy dependence of the $1_0^+ \rightarrow 0_0^+$ and $2_1^- \rightarrow 1_1^+$ de-excitation cross sections of o- and p-NH₃, respectively, in collision with p-H₂ ($j_2 = 0$), o-H₂ ($j_2 = 1$) and H.

Important resonance peaks appear with both H and H₂ colliders. This is related to the presence of an attractive potential well, which allows for bound and quasi-bound states to be formed before the complex dissociates. Both shape and Feshbach resonances are then expected (Ma et al. 2015).

The cross sections for collisions with o-H₂ ($j_2 = 1$) display smoother variations because of resonance overlaps. Indeed, for o-H₂ we expect a large number of quasi-bound states due to the contribution of an additional coupling terms $j+j_2=j_{12}$ absent in collisions with p-H₂ ($j_2 = 0$).

At low to intermediate energies, collisional cross sections with H₂ ($j_2 = 0, 1$) are larger than those with H. This reflects the deeper potential well of the NH₃-H₂ PES compared to that of the NH₃-H PES. Similarly, the NH₃-o-H₂ ($j_2 = 1$) cross sections are larger than the NH₃-p-H₂ ($j_2 = 0$) because of the permanent quadrupole moment of H₂, which vanishes for $j_2 = 0$ but not for $j_2 = 1$, leading to a stronger interaction of NH₃ with o-H₂ ($j_2 = 1$) than with p-H₂ ($j_2 = 0$).

As mentioned above, Ma et al. (2015) have also employed the PES of Maret et al. (2009) to compute inelastic cross sections for NH₃-H₂. We have compared our new results with those obtained by Ma et al. (2015) and both sets of cross sections were found to agree within a few percent, as expected.

3.2 Rate coefficients

In Figs. 2 and 3, de-excitation rate coefficients are presented for collisions of o- and p-NH₃ with H₂ and H.

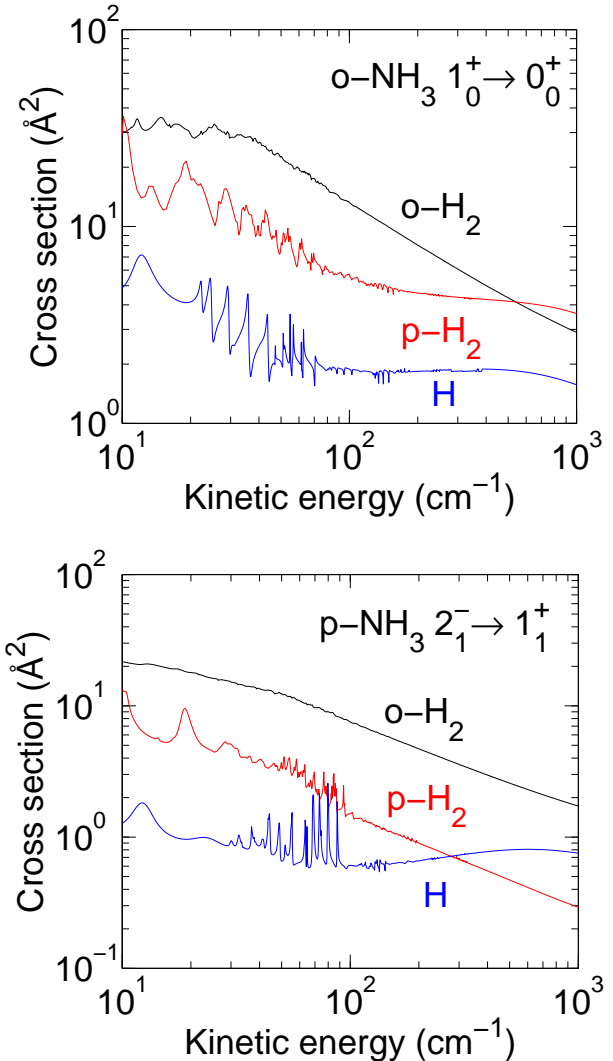


Figure 1. Rotational de-excitation cross sections of o- and p-NH₃ by p-H₂ ($j_2 = 0$) and o-H₂ ($j_2 = 1$) and H for the transitions $1_0^+ \rightarrow 0_0^+$ and $2_1^- \rightarrow 1_1^+$.

We observe a smooth temperature variation of the de-excitation rate coefficients that slightly increase with increasing temperature. As expected from the above discussion, the rate coefficients for collisions with o-H₂ ($j_2 = 1$) are larger than those for collisions with p-H₂ ($j_2 = 0$).

We now examine the collisional propensity rules. Figure 4 shows, at 100 K, the rotational de-excitation rate coefficients for transitions out of o-NH₃ ($j_k^e = 4_0^+$) and p-NH₃ ($j_k^e = 4_4^+$) due to collisions with H₂ ($j_2 = 0, 1$) and H. For o-NH₃ in its 4_0^+ state (upper panel), we notice a marked de-excitation propensity rules in favor of the 3_0^+ state ($\Delta j = 1$, $\Delta k = 0$ and symmetry conserving) and in favor of the 4_3^+ state ($\Delta j = 0$, $\Delta k = 3$, and symmetry conserving). For p-NH₃ in its 4_4^+ state (lower panel), the preferred transitions correspond to $\Delta k = 3$, since there is no de-excitation with $\Delta k = 0$ for this initial level. No propensity on the symmetry (or parity) index is observed. As can be seen from Fig. 4, the same general trends are observed for the three different colliders p-H₂ ($j_2 = 0$), o-H₂ ($j_2 = 1$) and H, although propen-

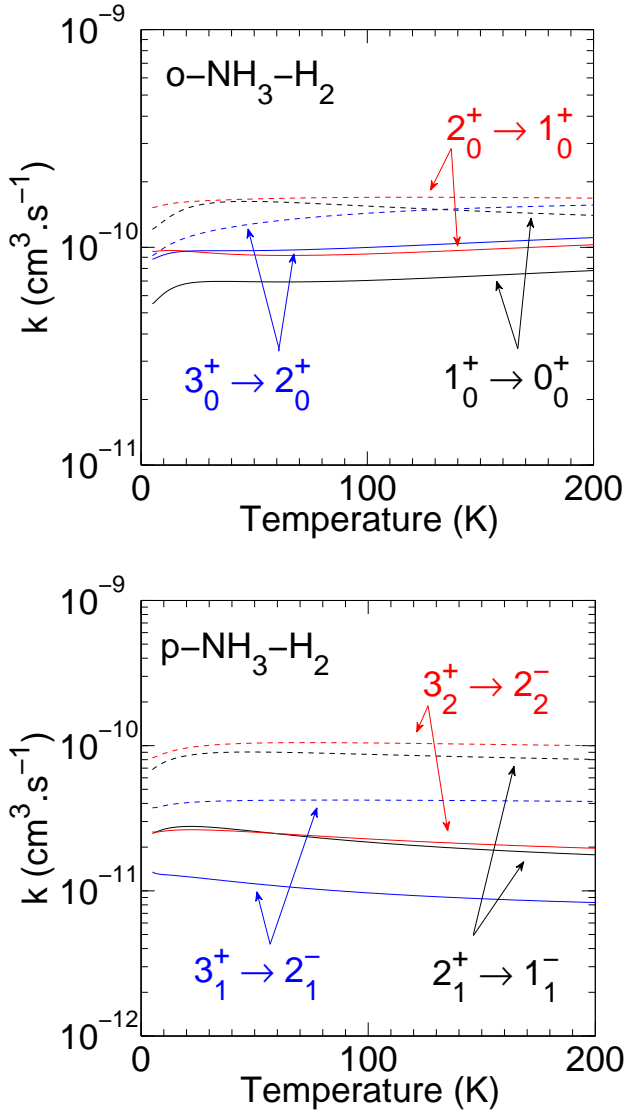


Figure 2. Thermal dependence of the rate coefficients of o - and $p\text{-NH}_3$ by $p\text{-H}_2$ ($j_2=0$) (solid line) and $o\text{-H}_2$ ($j_2=1$) (dashed line) for a set of transitions with $\Delta j = 1$.

sities tend to weaken in the case of $o\text{-H}_2$ ($j_2=1$) due to the additional angular couplings. To summarize, collisional transitions are found to favor transitions with $\Delta j = 0, \pm 1, \pm 2$ and $\Delta k = 0, \pm 3$ with no clear propensity on the symmetry (or parity) index. This can be compared to the radiative (dipolar) selection rules which obey $\Delta j = 0, \pm 1$, $\Delta k = 0$ and parity changing.

3.3 Comparison with previous data

In astrophysical applications, it is usual to infer the rate coefficients of a colliding system from the values calculated for a closely related system (i.e. same target but with different collisional partners), using a scaling factor coefficient such as the square root of the reduced mass ratio (i.e. assuming identical cross sections for the two colliders).

In order to assess the validity of such a simple scaling law, we compare in Fig. 5 the current rate coefficients of

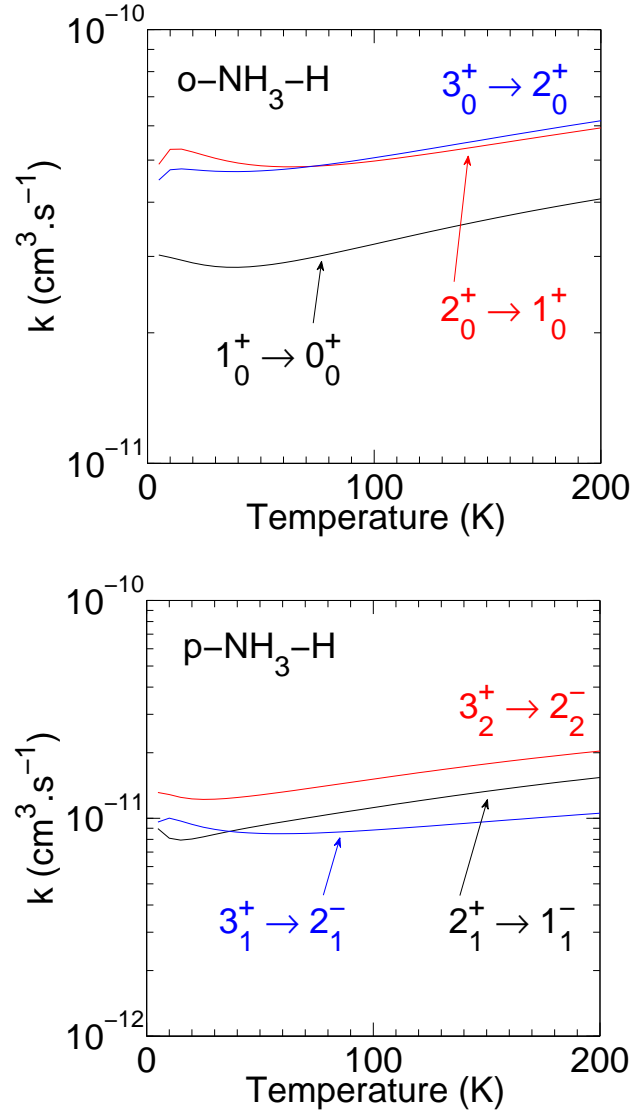


Figure 3. Thermal dependence of the rate coefficients of o - and $p\text{-NH}_3$ by H for a set of transitions with $\Delta j = 1$.

both o - and $p\text{-NH}_3$ in collision with H_2 , H and those obtained by Maret et al. (2009) and Machin & Roueff (2005) for the spherical $p\text{-H}_2$ ($j_2=0$) and He colliders, respectively. Assuming the (reduced mass) scaling law is valid, the rate coefficients for $p\text{-H}_2$ ($j_2=0$) and H should be about 50% and 80% larger than the He rate coefficients, respectively, owing to the smaller collisional reduced masses. However, as expected and found for many other hydrides like HCl (Lanza et al. 2014), H_2O (Daniel, Cernicharo & Dubernet 2006), etc. it can be seen in Fig. 5 that the rate coefficient ratios vary significantly with both the temperature and the transition considered. The rate coefficients for H_2 (both o - and $p\text{-H}_2$) are up to two orders of magnitude larger than those for He (Machin & Roueff 2005). The rate coefficients for collisions with H are not larger than those with $p\text{-H}_2$ ($j_2=0$), contrary to what could be anticipated from the (reduced mass) scaling law. The differences between the three colliders are most pronounced at low temperature and can be explained by the fact that at low collisional energy,

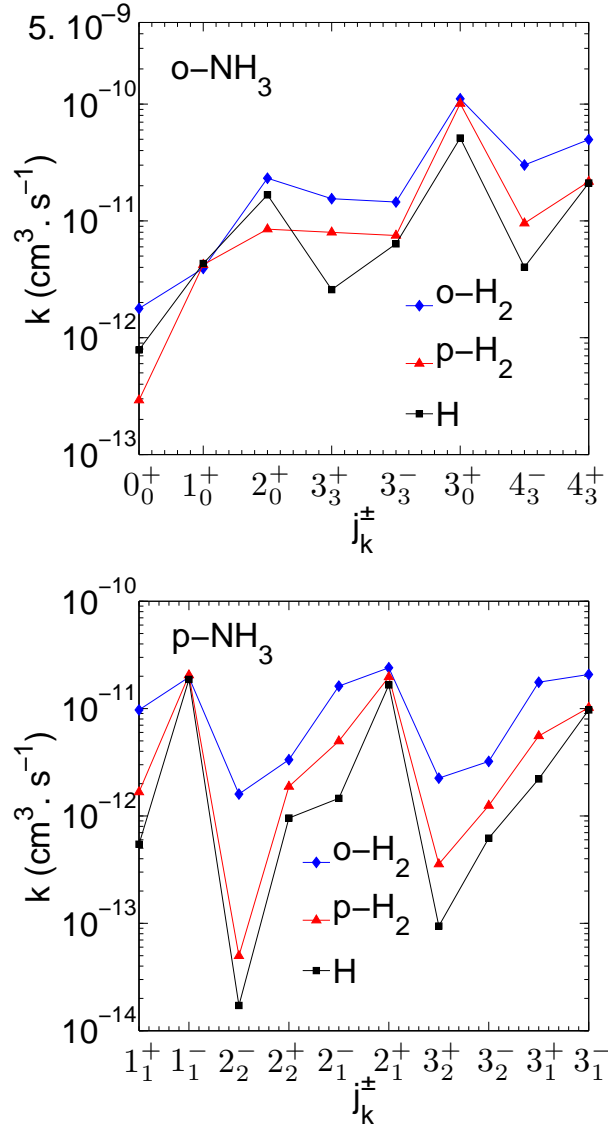


Figure 4. Rate coefficients for transitions out of the initial NH_3 states $j_k^\epsilon = 4_0^+$ (upper panel) and $j_k^\epsilon = 4_4^+$ (lower panel) due to collisions with $\text{p-H}_2(j_2=0)$, $\text{o-H}_2(j_2=1)$ and H at $T=100$ K.

cross sections are very sensitive to the well depth of the PES. Here, the well depth is 3 and 8 times larger for H_2 than for H and He (-267 cm^{-1} vs. -78.31 cm^{-1} and -32.85 cm^{-1} , respectively). As a result, we confirm that, for hydrides, He atoms are very poor substitutes for H or H_2 .

Regarding the rate coefficients for p-H_2 , we can notice significant differences (up to a factor of 2) between the present calculations and those of Maret et al. (2009) (see Fig.5, upper panel). We recall that these differences reflect the inclusion of the rotational (non-spherical) structure of p-H_2 in our treatment. However, on the average, the differences are less than 30% and the temperature variation of the two sets of data is quite similar. Hence, we do not expect a major impact of the new $\text{p-H}_2(j_2=0)$ rate coefficients on the astrophysical modelling. Additionally, as pointed out in our previous figures, we observe again in Fig. 5 a large difference between p- and o-H_2 . It is thus crucial to consider the two nuclear spin species of H_2 as two distinct colliders.

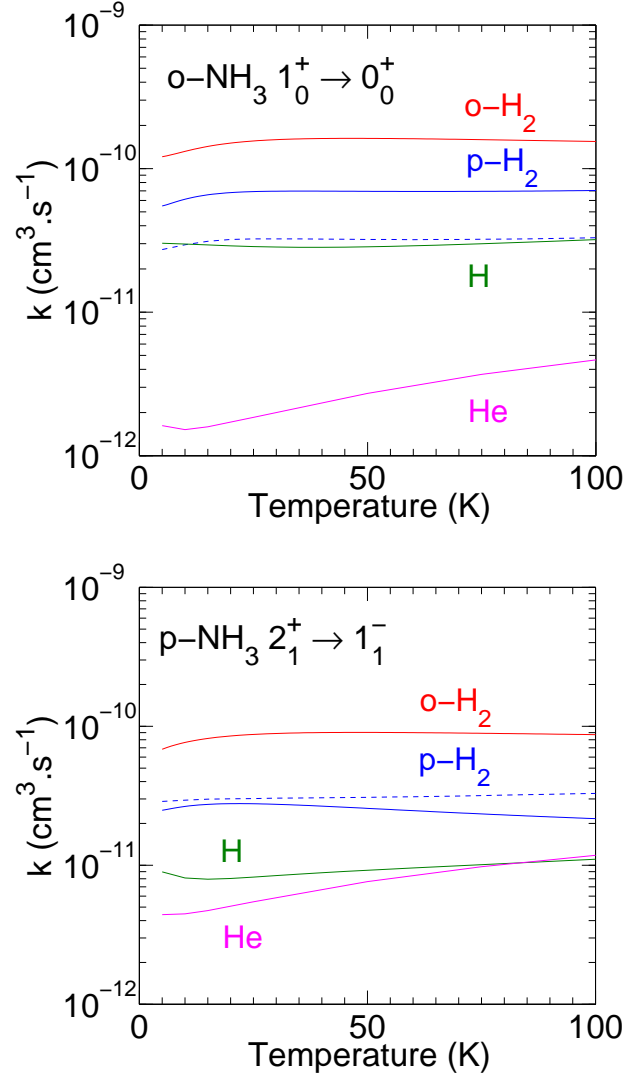


Figure 5. Comparison between the rate coefficients for collisional de-excitation of o- and p-NH_3 by H , o-H_2 and p-H_2 (dashed line for the rate coefficients of Maret et al. (2009)) and He (from Machin et al. (2005)).

The whole set of rotation-inversion rate coefficients for $\text{p-H}_2(j_2=0)$, $\text{o-H}_2(j_2=1)$ and H will be available through the LAMDA (Schöier et al. 2005) and BASECOL (Dubernet et al. 2013) data bases. We note that in some environments the fraction of $\text{p-H}_2(j_2=2)$ can become significant, e.g. at kinetic temperatures above ~ 100 K. We have found that cross sections for H_2 initially in $j_2=2$ differ by less than 30% with those for H_2 in $j_2=1$ (see also Daniel et al. (2014) for NH_2D). As a result, it can be assumed that rate coefficients for $\text{p-H}_2(j_2=2)$ are identical to those for $\text{o-H}_2(j_2=1)$.

4 THE AMMONIA THERMOMETER

Because radiative dipolar transitions with $\Delta k \neq 0$ are forbidden in NH_3 (except for very slow $\Delta k = \pm 3$ transitions), the exchange of population between the different k -

ladders occurs essentially via collisional processes. For many years, the inversion transitions for different k -ladders at ~ 20 -30 GHz have been employed to derive kinetic temperatures in both cold (< 40 K) and warm (> 100 K) galactic and extra-galactic star formation environments. The $(1_1^- \rightarrow 1_1^+)/ (2_2^+ \rightarrow 2_2^-)$ line ratio, in particular, has been widely used to monitor the lowest kinetic temperatures (< 40 K). Considering only the first three doublets 1_1^\pm , 2_2^\pm and 2_1^\pm and assuming that the population of the 2_1^\pm doublet is negligible relative to that in 1_1^\pm , Walmsley & Ungerechts (1983) have shown that the excitation temperature between the two lowest doublets is given by the analytical formula:

$$T_{1,2}^A = T_k \left\{ 1 + \frac{T_k}{T_0} \ln \left[1 + \frac{k(2_2 \rightarrow 2_1)}{k(2_2 \rightarrow 1_1)} \right] \right\}^{-1} \quad (2)$$

where T_0 is the energy difference between the first two metastable doublets (41.2 K), T_k is the kinetic temperature and $k(2_2 \rightarrow 2_1)$ and $k(2_2 \rightarrow 1_1)$ are the rotational rate coefficients (i.e. averaged and summed over the inversion symmetry index). In practice, this formula is accurate at temperatures below 40 K and at densities lower than 10^5 cm^{-3} . We note that analytic expressions can be derived also for higher metastable levels (Walmsley & Ungerechts 1983).

Observationally, $T_{1,2}$ is determined by observing the hyperfine components of the $1_1^- \rightarrow 1_1^+$ and $2_2^+ \rightarrow 2_2^-$ inversion transitions. The inversion doublets have indeed hyperfine components due to (mainly) the quadrupole moment of the ^{14}N nucleus. Assuming the excitation temperature of each hyperfine transition (within a doublet) is the same, one can derive the opacities $\tau(1_1)$ and $\tau(2_2)$ from which the excitation temperature $T_{1,2}$ can be obtained (Ho et al. 1979; Juvela et al. 2012). In order to derive the kinetic temperature from the measured $T_{1,2}$ excitation temperature, one needs to calibrate the ammonia thermometer, Eq. (2), and a very good knowledge of the collisional rate coefficients is necessary.

Maret et al. (2009) have investigated the robustness of the ammonia thermometer by comparing the excitation temperature $T_{1,2}$ computed using their rate coefficients with that computed using the older collisional data of Danby et al. (1988). Although the rotation-inversion rate coefficients differ by up to a factor of 2, they found almost identical excitation temperatures $T_{1,2}$ (see their Fig. 5) and concluded that the rate coefficients of Danby et al. (1988) were of sufficient accuracy to calibrate the thermometer.

Here we test for the first time the impact of including the H_2 rotational structure on the ammonia thermometer. In Fig. 6, the ratio of the rate coefficients $k(2_2 \rightarrow 2_1)$ and $k(2_2 \rightarrow 1_1)$ is plotted as function of temperature. We first observe that this ratio is lower than unity whatever the collider. We notice that the inclusion of $j_2 = 2$ in the H_2 basis set (neglected in Maret et al. (2009)) tends to increase the ratio by up to 10%. The difference between o- and p- H_2 rate coefficients is even more significant, with up to a 30% increase of the ratio at 40 K. Finally, the collisions with hydrogen atoms give the lowest ratio. These differences reflect small variations in propensity rules, as illustrated in Fig. 4.

The different ratios plotted in Fig. 6 translate into different excitation temperatures $T_{1,2}$, as shown in Fig. 7. In this plot, we can first notice that for small kinetic temperature (< 10 K), e.g. in cold prestellar cores, $T_{1,2} = T_k$ and $T_{1,2}$ can be used as a direct proxy for the kinetic temper-

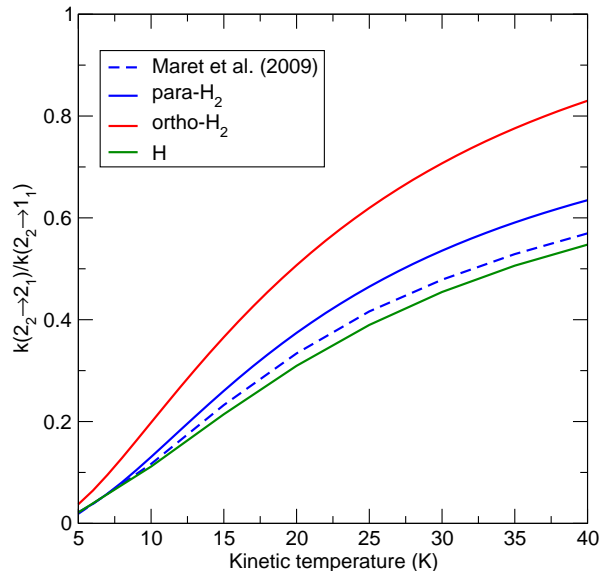


Figure 6. Ratio of the rate coefficients $k(2_2 \rightarrow 2_1)$ and $k(2_2 \rightarrow 1_1)$ as function of the kinetic temperature.

ature. Deviations between $T_{1,2}$ and T_k occur above 10 K. As expected, the difference between the present results for p- H_2 and those of Maret et al. (2009) is small and does not exceed 1 K. Indeed the logarithm in Eq. (1) further reduces the differences observed in Fig. 6. We also provide the excitation temperatures $T_{1,2}$ for a normal- H_2 gas, i.e. with an H_2 OPR of 3, and for a purely atomic gas. The differences with p- H_2 are found to be less than 2 K, suggesting that the ammonia thermometer cannot be employed to provide indirect constraints on the H_2 OPR or on the atomic fraction of the gas. Indeed, the three calibration curves agree within 2 K and any estimate of the relative abundance of o- H_2 , p- H_2 and H from the measured $T_{1,2}$ would require the knowledge of T_k with a sub-Kelvin accuracy, which is hardly achievable with the current precision of observations.

Finally, in order to provide a useful calibration of the ammonia thermometer for dark clouds and starless cores, we fitted the ratio of the rate coefficients $k(2_2 \rightarrow 2_1)$ and $k(2_2 \rightarrow 1_1)$ in the case of p- $\text{H}_2(j_2 = 0)$. Indeed, although H_2 cannot be directly observed at low temperature, indirect observations indicate that the cold interstellar gas is mainly composed by p- $\text{H}_2(j_2 = 0)$, with an OPR lower than 1% below ~ 30 K (Troscompt et al. 2009; Paganì et al. 2009; Faure et al. 2013). From the results plotted in Fig. 6 we have derived:

$$\frac{k(2_2 \rightarrow 2_1)}{k(2_2 \rightarrow 1_1)} = 1.073 \exp(-21.01/T_k), \quad (3)$$

which has an accuracy better than 2% above 10 K (remember $T_k = T_{1,2}$ below 10 K). This fit can be used to relate the kinetic temperature T_k to $T_{1,2}$ via Eq. (2), provided that $T_k < 40$ K. We also fitted the reverse relation and obtained:

$$T_k = T_{1,2} \left\{ 1 - \frac{T_{1,2}}{T_0} \ln [1 + 1.608 \exp(-25.25/T_{1,2})] \right\}^{-1}, \quad (4)$$

which has an accuracy better than 0.3%. We note that this analytical formula was suggested by Tafalla et al. (2004)[see their Appendix B]. Their numerical expression was based on the rate coefficients of Danby et al. (1988) and, as expected,

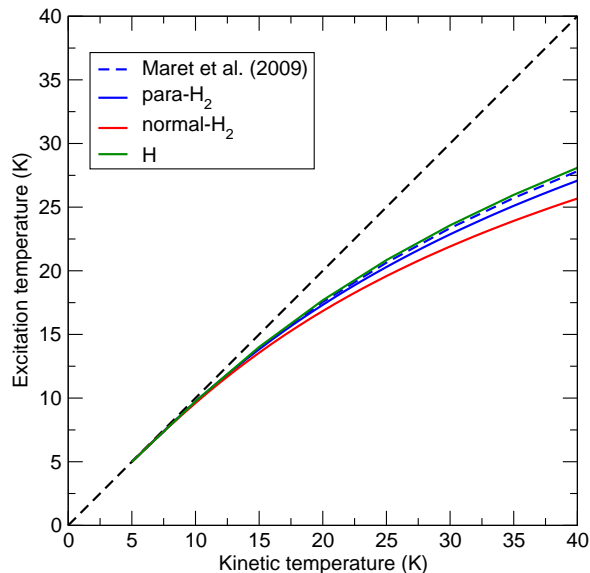


Figure 7. Excitation temperature between the 1_1 and 2_2 metastable levels of p-NH₃ as function of the kinetic temperature. The analytic expression, Eq. (1), is employed with the rate coefficients computed in this study and from the rate coefficients of Maret et al. (2009) for p-H₂. The dashed straight line corresponds to $T_k = T_{1,2}$.

the two expressions agree within 1 K in the temperature range $T_k=1-40$ K. Eq. (4) can be employed confidently to derive T_k at temperatures lower than 40 K and for densities smaller than 10^5 cm⁻³. For higher densities and temperatures, high-lying k -ladders (above the level 2_1) play a role and it is necessary to solve the statistical equilibrium equations within a radiative transfer treatment, which is beyond the scope of the present paper.

5 CONCLUSION

We have presented rotation-inversion (de)excitation rate coefficients for p- and o-NH₃ due to collisions with p-H₂ ($j_2 = 0$), o-H₂ ($j_2 = 1$) and H. The scattering calculations were performed using the interaction potential described in Maret et al. (2009) for NH₃-H₂ and in Li & Guo (2014) for NH₃-H. The lowest 17 and 34 rotational levels of o- and p-NH₃, respectively, were considered and rate coefficients were computed for kinetic temperatures up to 200 K. The new rate coefficients for p-H₂ were found to agree within a factor of 2 (30% on average) compared to the older computations of Maret et al. (2009). Our calculations complete the available sets for the ammonia molecule: specific calculations are now available for the dominant neutral colliders of the interstellar medium, i.e. p-H₂, o-H₂, H (this work) and He (Machin et al. 2005).

We note that the hyperfine structure of NH₃ is resolved in some astrophysical spectra. In order to model such observations, hyperfine selective rate coefficients are necessary. The accurate recoupling theory (see e.g. Faure & Lique (2012)) should be therefore extended to the case of molecule-molecule collisions, as in Lanza et al. (2014) for the HCl-H₂ system. The statistical method (in which the hyperfine selective rate coefficients are taken to be proportional to the

statistical weights of the final states) can be also employed as a simple approximation. It should be noted, however, that the statistical approach is known to be insufficient in some cases, as discussed by Stutzki & Winnewisser (1985) and, more recently, by Faure & Lique (2012).

We note also that the present rotation-inversion rate coefficients for the main ammonia isotopologue ¹⁴NH₃ can be safely employed for the ¹⁵NH₃ isotopologue because the ¹⁴N/¹⁵N isotopic effect is negligible. In contrast, a hydrogen/deuterium substitution has a great impact since *i*) the principal moment of inertia axes are rotated (except in ND₃) and *ii*) the shift of the centre of mass is significant. Rotational rate coefficients were computed recently for all deuterated ammonia isotopologues (Daniel et al. 2014, 2016) so that collisional data are indeed now available for all ammonia isotopologues.

Finally, future studies will address the excitation of higher rotational levels, at higher temperatures, as well as the excitation of the vibrational levels of ammonia (the lowest one opens at 950 cm⁻¹). This will require a full twelve-dimensional NH₃-H₂ PES.

ACKNOWLEDGEMENTS

This work has been supported by the Agence Nationale de la Recherche (ANR-HYDRIDES), contract ANR-12-BS05-0011-01.

REFERENCES

- Bouhafs N., Lique F., Faure A., Bacmann A., Li J., Guo H., 2017, *The Journal of Chemical Physics*, 146, 064309
- Cheung A. C., Rank D. M., Townes C. H., Thornton D. D., Welch W. J., 1968, *Phys. Rev. Lett.*, 21, 1701
- Danby G., Flower D. R., Kochanski E., Kurdi L., Valiron P., 1986, *J. Phys. B At. Mol. Opt. Phys.*, 19, 2891
- Danby G., Flower D. R., Valiron P., Schilke P., Walmsley C. M., 1988, *MNRAS*, 235, 229
- Daniel F., Cernicharo J., Dubernet M., 2006, *ApJ*, 648, 461
- Daniel F., Faure A., Wiesenfeld L., Roueff E., Lis D. C., Hily-Blant P., 2014, *MNRAS*, 444, 2544
- Daniel F. et al., 2016, *MNRAS*, 457, 1535
- Dubernet M. L. et al., 2013, *A&A*, 553, A50
- Faure A., Hily-Blant P., Le Gal R., Rist C., Pineau des Forêts G., 2013, *ApJ*, 770, L2
- Faure A., Lique F., 2012, *MNRAS*, 425, 740
- Green S., 1976, *J. Chem. Phys.*, 64, 3463
- Gubbels K. B., van de Meerakker S. Y. T., Groenenboom G. C., Meijer G., van der Avoird A., 2012, *J. Chem. Phys.*, 136, 074301
- Ho P. T. P., Barrett A. H., Myers P. C., Matsakis D. N., Chui M. F., Townes C. H., Cheung A. C., Yngvesson K. S., 1979, *ApJ*, 234, 912
- Ho P. T. P., Townes C. H., 1983, *ARA&A*, 21, 239
- Hodges M. P., Wheatley R. J., 2001, *J. Chem. Phys.*, 114, 8836
- Hutson J. M., Green S., 1994. MOLSCAT computer code, version 14 (1994), distributed by Collaborative Computational Project No. 6 of the Engineering and Physical Sciences Research Council (UK)

- Juvela M., Harju J., Ysard N., Lunttila T., 2012, *A&A*, 538, A133
- Lanza M., Kalugina Y., Wiesenfeld L., Lique F., 2014, *Journal of Chemical Physics*, 140, 064316
- Le Gal R., Hily-Blant P., Faure A., Pineau des Forêts G., Rist C., Maret S., 2014, *A&A*, 562, A83
- Li J., Guo H., 2014, *Physical Chemistry Chemical Physics*, 16, 6753
- Ma Q., van der Avoird A., Loreau J., Alexander M. H., van de Meerakker S. Y. T., Dagdigian P. J., 2015, *J. Chem. Phys.*, 143, 044312
- Machin L., Roueff E., 2005, *J. Phys. B At. Mol. Opt. Phys.*, 38, 1519
- Maret S., Faure A., Scifoni E., Wiesenfeld L., 2009, *MNRAS*, 399, 425
- Mladenović M., Lewerenz M., Cilpa G., Rosmus P., Cham-
baud G., 2008, *Chemical Physics*, 346, 237
- Offer A., Flower D. R., 1989, *Journal of Physics B Atomic
Molecular Physics*, 22, L439
- Oka T., 1967, *J. Chem. Phys.*, 47, 4852
- Pagani L. et al., 2009, *A&A*, 494, 623
- Persson C. M. et al., 2010, *A&A*, 521, L45
- Persson C. M. et al., 2012, *A&A*, 543, A145
- Pirani F. a., Cappelletti D., Belpassi L., Tarantelli F., 2013, *J. Phys. Chem. A*, 117, 12601
- Rist C., Alexander M. H., Valiron P., 1993, *J. Chem. Phys.*, 98, 4662
- Rist C., Faure A., 2012, *Journal of Mathematical Chem-
istry*, 50, 588
- Schleipen J., ter Meulen J. J., 1991, *Chem. Phys.*, 156, 479
- Schöier F. L., van der Tak F. F. S., van Dishoeck E. F.,
Black J. H., 2005, *A&A*, 432, 369
- Sheppelman J. P., Smizaski G. W., Curotto E., Mella M.,
2012, *Chemical Physics Letters*, 535, 49
- Stutzki J., Winnewisser G., 1985, *A&A*, 144, 1
- Surin L. A., Tarabukin I. V., Schlemmer S., Breier A. A.,
Giesen T. F., McCarthy M. C., van der Avoird A., 2017, *ApJ*, 838, 27
- Tafalla M., Myers P. C., Caselli P., Walmsley C. M., 2004, *A&A*, 416, 191
- Tkáč O., Saha A. K., Loreau J., Ma Q., Dagdigian P. J.,
Parker D. H., van der Avoird A., Orr-Ewing A. J., 2015, *Molecular Physics*, 113, 3925
- Tkáč O. et al., 2014, *Phys. Chem. Chem. Phys.*, 16, 477
- Troscompt N., Faure A., Maret S., Ceccarelli C., Hily-Blant
P., Wiesenfeld L., 2009, *A&A*, 506, 1243
- Walmsley C. M., Ungerechts H., 1983, *A&A*, 122, 164
- Willey D. R., Timlin, Jr. R. E., Merlin J. M., Sowa M. M.,
Wesolek D. M., 2002, *ApJS*, 139, 191

This paper has been typeset from a $\text{\TeX}/\text{\LaTeX}$ file prepared by the author.